




Ultrafast dissociation dynamics of singly and doubly ionized N_2O in strong laser fields

Xinning Zhao, Xitao Yu , Xinpeng Xu, Zhongyu Yin, Jiaqi Yu, Xiaokai Li, Pan Ma, Dongdong Zhang, Chuncheng Wang, Sizuo Luo ,* and Dajun Ding [†]
Institute of Atomic and Molecular Physics, Jilin University, Changchun 130012, China



(Received 17 October 2019; published 10 January 2020)

We study the ultrafast dissociation of singly and doubly ionized N_2O molecules using strong IR-laser pump and IR-laser probe techniques in combination with the three-body ($\text{N}^+ + \text{N}^+ + \text{O}^+$) coincidence measurement. Two time-dependent kinetic energy release bands are observed and assigned as ultrafast evolutions after further ionization of N_2O^+ and N_2O^{2+} . The real-time bond stretching and structure bending are observed from N_2O^+ populated on the $B^2\Pi$ state, and the kinetic energy correlation between N^+ and O^+ ions reveals that the concerted fragmentation dominates while the contribution of sequential fragmentation increases with time. Two two-body and two three-body fragmentation pathways of N_2O^{2+} are assigned, and the ultrafast dissociation processes are tracked by measuring the time-dependent Dalitz distributions and kinetic energy correlations between N^+ and O^+ ions.

DOI: [10.1103/PhysRevA.101.013416](https://doi.org/10.1103/PhysRevA.101.013416)

I. INTRODUCTION

Tracking the evolution of molecular structures after interaction with ultrafast laser pulses, such as vibration, bond breaking, and isomerization, by taking advantage of ultrashort laser pulses and advanced particle detection technology will promote our understanding of light-matter interaction as well as improve the ability to control chemical reactions [1–5]. Strong field ionization of molecules, which launches a vibrational wave packet of molecular cations, has been extensively studied using pump-probe methods in recent years [4–9]. The vibrational wave packet has been tracked by measuring momenta of fragment ions, and the multimode coherence of vibrational states has been observed by measuring XUV absorption spectra in real time [8,9]. Moreover, the bond breaking which occurs when a molecular cation is populated to dissociative states from strong field ionization can be tracked by measuring the time-dependent kinetic energy release (KER) of fragments as well as the yield of fragment ions [10–13]. The Coulomb explosion (CE) after multielectron ionization is an effective method to image the shape of molecules, and the nuclear movement of molecules has been recorded using time-resolved Coulomb explosion imaging (CEI) with the help of the pump-probe scheme [6,7,14,15].

It is well known that N_2O^+ is the intermediate product of the very important reaction $\text{O}^+ + \text{N}_2 \rightarrow \text{NO}^+ + \text{N}$ in the upper ionosphere of our earth [16,17]. The dissociation and predissociation dynamics of N_2O^+ have been extensively studied both experimentally and theoretically [18–22]. The valence electronic configuration of N_2O is $(1\sigma)^2(2\sigma)^2(3\sigma)^2(4\sigma)^2(5\sigma)^2(6\sigma)^2(1\pi)^4(7\sigma)^2(2\pi)^4$, and the cation N_2O^+ will be populated on $X^2\Pi$, $A^2\Sigma^+$, $B^2\Pi$, and

$C^2\Sigma^+$ states after removing the corresponding 2π , 7σ , 1π , and 6σ electrons [22]. The ground state $X^2\Pi$ of N_2O^+ is stable, while molecular cations on $A^2\Sigma^+$, $B^2\Pi$, and $C^2\Sigma^+$ states can predissociate. Three predissociation pathways of the $A^2\Sigma^+$ state have been identified with lifetimes of vibrational states in $A^2\Sigma^+$ ranging from tens to hundreds of nanoseconds [20–22]. Three fragments NO^+ , N_2^+ , and O^+ can be produced from dissociation of $B^2\Pi$ states [22]. Furthermore, the lifetime of the $B^2\Pi$ state has been deduced from two-photon absorption spectroscopy to be 30 fs [23]. The involved dissociation pathways and lifetime (~ 2 ps) of $C^2\Sigma^+$ have been identified by ion-electron coincidence measurements [24]. The non-Born-Oppenheimer dynamics of highly excited states of N_2O^+ and the bond cleavage dynamics of N_2O^{2+} have been tracked in an EUV pump and IR probe measurement [25]. The CE of N_2O^{2+} in strong laser fields has also attracted significant experimental attention [26,27]. The directional emission of ions in the denitrogenation ($\text{N}^+ + \text{NO}^+$) and deoxygenation ($\text{N}_2^+ + \text{O}^+$) explosion channels of the dication has been controlled by steering the electric field of nearly-single-cycle laser pulses [27]. Recently, the bond-breaking dynamics of N_2O^{2+} triggered by an EUV pulse has been probed by a time-delayed near-IR pulse. In addition, the two-body and three-body cleavage dynamics on a femtosecond timescale have been tracked and the influence of concerted and sequential fragmentation during double ionization was discussed in Ref. [28].

In this work the nuclear dynamics triggered by strong field ionization are probed by the time-resolved CEI method. The time-dependent three-body coincidence measurement ($\text{N}_2\text{O}^{3+} \rightarrow \text{N}^+ + \text{N}^+ + \text{O}^+$) reveals the ultrafast structural deformation and the dissociation of N_2O^+ and N_2O^{2+} . This experiment demonstrates that the time-resolved coincidence measurement is a valuable way to monitor the structure evolution and dissociation dynamics of molecules on the femtosecond timescale.

*luosz@jlu.edu.cn

[†]dajund@jlu.edu.cn

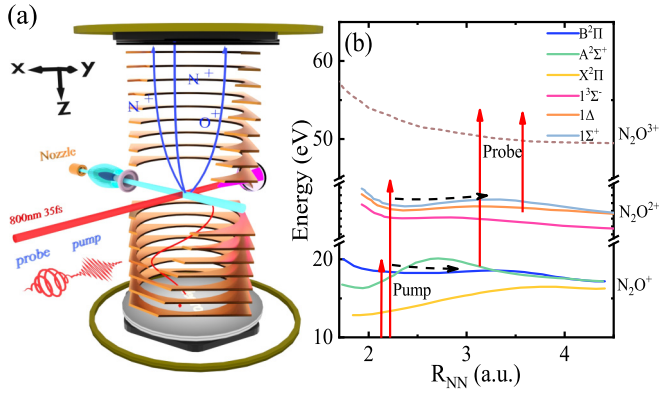


FIG. 1. (a) Schematic illustration of the experimental setup. A pump-probe setup with linearly and elliptically polarized laser pulses is built to track the ultrafast dissociation dynamics of molecules. For positive delays, the pump and probe lasers are linearly and elliptically ($\varepsilon \sim 0.7$) polarized with intensities of 1.0×10^{14} and 3.5×10^{14} W/cm², respectively. For negative delays, the pump and probe pulses exchange roles. (b) Schematic representation of the pump-probe evolution of N₂O⁺ and N₂O²⁺. The relevant potential energy curves of N₂O⁺ and N₂O²⁺ molecule are adopted from Refs. [22,31].

II. EXPERIMENTAL METHOD

Our experiment setup includes a pump-probe laser system and a cold target recoil ion momentum spectrometer (COLTRIMS) [29,30] as illustrated in Fig. 1(a). The femtosecond laser beam (800 nm, 1 kHz, ~ 35 fs) generated from a chirped pulse amplified Ti:sapphire system is used to study the ultrafast dissociation dynamics of molecules. In order to disentangle the ionization and dissociation of molecules, a linearly polarized laser (1.0×10^{14} W/cm²) and an elliptically polarized laser (3.5×10^{14} W/cm², $\varepsilon \sim 0.7$) are chosen as the pump and probe lasers. The polarization direction of the linearly polarized laser and the major axis of the elliptically polarized laser are parallel to the y axis and the minor axis of the elliptically polarized laser is parallel to the z axis as shown in Fig. 1(a). The pump and probe lasers are recombined after passing through a Mach-Zehnder interferometer and then are sent and focused into the COLTRIMS machine. The pump laser ionizes N₂O molecules in the supersonic gas jet and populates molecules to ionic states (N₂O⁺ and N₂O²⁺) as shown in Fig. 1(b). The relevant potential energy curves of N₂O⁺ and N₂O²⁺ are adopted from previous studies [22,31]. The probe laser further ionizes the samples to N₂O³⁺, which is unstable and breaks up into N⁺ + N⁺ + O⁺. The time delay between pumping and probing lasers is controlled by moving a delay stage. The zero time delay of two laser pulses is determined by measuring the time-dependent N₂O⁺ signal, and the full width at half maximum of the cross correlation profile is 90 fs determined, from a Gaussian fitting. The produced ions are extracted and projected to a time- and position-sensitive detector by a weak homogeneous electric field. The mass-to-charge ratio and three-dimensional momentum distribution of the ions are calculated from the measured time and position information. More details of the experimental setup can be found in our previous publications [32,33]. Here we focus on quantitative analysis of the ions (N⁺ + N⁺ + O⁺) from the

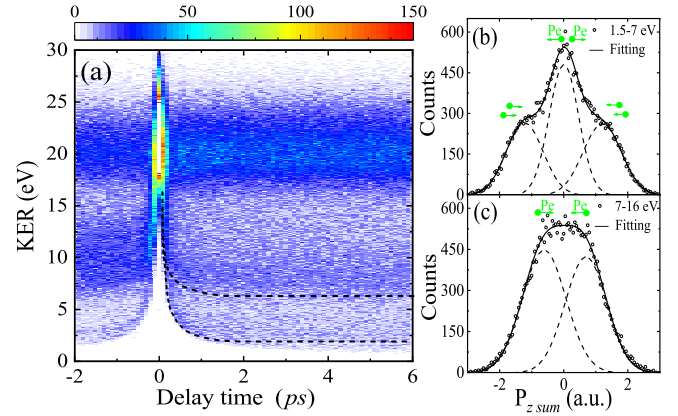


FIG. 2. (a) Pump-probe delay dependence of the KER for the three-body CE channel N⁺ + N⁺ + O⁺ from further ionization of N₂O⁺ and N₂O²⁺. Two dashed lines are added to visualize the time dependence of KERs for two dissociation channels. Also shown are the corresponding ion sum-momentum distributions $P_{z\text{sum}}$ for (b) the low-KER band (1.5–7.0 eV) and (c) the high-KER band (7.0–16.0 eV).

CE of triply charged final states. The events that meet the condition $|p_{z,\text{ion1}} + p_{z,\text{ion2}} + p_{z,\text{ion3}}| < 3$ a.u. are chosen as a criterion for coincident event identification. In order to reduce the time jitter between two laser pulses, we scan the delay from -2 to 6 ps in steps of 33.3 fs every 10 min and repeat the scan to collect enough data for analysis.

III. RESULTS AND DISCUSSION

The measured time-dependent KER from the three-body CE channel of N₂O³⁺ \rightarrow N⁺ + N⁺ + O⁺ is shown in Fig. 2(a). The positive delay time corresponds to the case that the linearly polarized laser is set as the pump and the elliptically polarized laser as the probe. Two characteristic features appear on the time-dependent KER spectra shown in Fig. 2(a). One is the strong delay-independent KER band in the energy regime between 17 and 25 eV and the second shows two delay-dependent KER bands with energies between 1.5 and 7 eV (low-KER channel) and 7 and 16 eV (high-KER channel) marked by black dash-dotted lines in the figures. The delay-independent KER band can be assigned as the direct triple ionization of N₂O from the pump or probe laser only. Two time-dependent KER bands evolve towards lower KER with increasing pump-probe time delay, which means molecules are populated in the dissociative states after strong field ionization and result in bond breaking as time goes on. The KER obtained from the CE decreases as the distance between fragments increases because the KER scales with $1/R$, where R is the separation between the fragment ions at the time of the further ionization. The measured time-dependent KER spectra show a fast decrease in the first 500 fs followed by a slow decrease in the next few picoseconds for the low-KER channel, while the high-energy channel shows a fast decay to around 8 eV in the first 200 fs and maintains a constant value from then on. The observations indicate that these two KER channels are generated from different dissociative states.

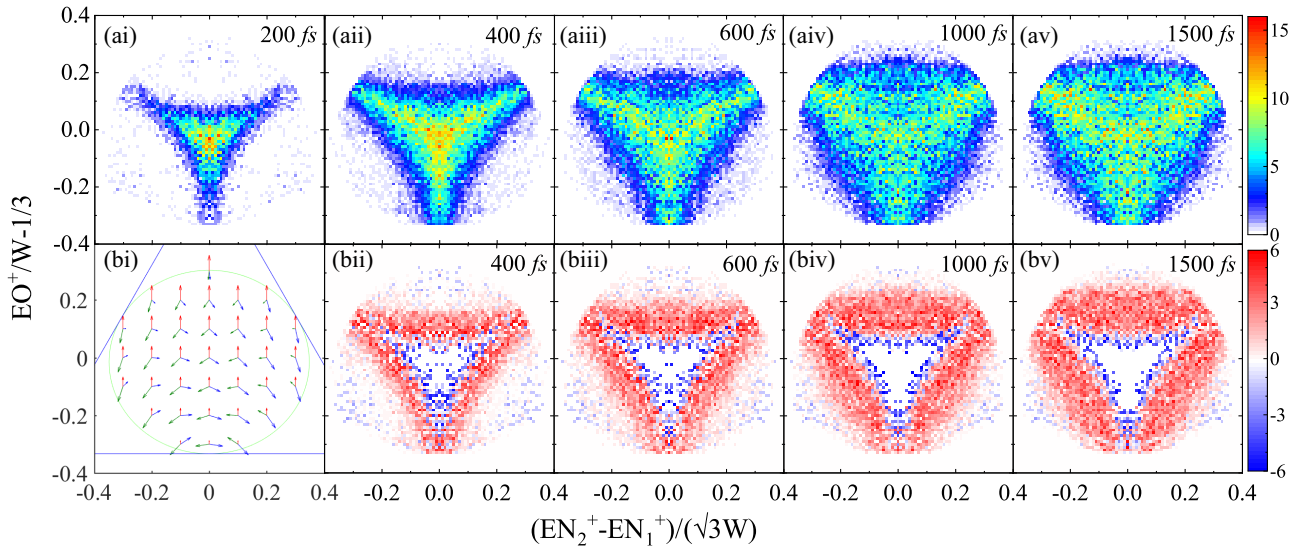


FIG. 3. Dalitz plot representation from the further ionization and dissociation of N_2O^+ into $\text{N}^+ + \text{N}^+ + \text{O}^+$ obtained after selecting the total KER from 1.5 to 7 eV at delay times of (a i) 200 fs, (a ii) 400 fs, (a iii) 600 fs, (a iv) 1000 fs, and (a v) 1500 fs. (b i) Corresponding Dalitz plot mapping of the three-body momenta. Also shown are the plots of the corresponding Dalitz distribution after subtracting the distribution at $\Delta t = 200$ fs at delay times of (b ii) 400 fs, (b iii) 600 fs, (b iv) 1000 fs, and (b v) 1500 fs. All the data are normalized to the integral before subtracting.

The KER-dependent ion sum momentum distributions of $\text{N}^+ + \text{N}^+ + \text{O}^+$ reveal the ionization process because the sum momentum of ions is equal to the sum momentum of electrons $p_{z\text{sum}} = p_{z\text{N}^+} + p_{z\text{N}^+} + p_{z\text{O}^+} = p_{ze1} + p_{ze2} + p_{ze3}$ according to the momentum conservation [34–36]. In the positive delay range, the ion sum momentum along the Z axis $p_{z\text{sum}}$ has a three-peak distribution for the low-KER channel as shown in Fig. 2(b); the three-peak structure of $p_{z\text{sum}}$ reflects the process of sequentially releasing two electrons in the elliptically polarized laser fields [35,36]. The electron is mainly ionized when the laser field points along the major axis (y axis), which ends with a final momentum along the minor axis (z axis) due to the angular streaking of the rotating laser fields [34,35]. The center peak comes from the process that two electrons are ejected in the opposite direction and two side peaks correspond to two electrons being ejected in the same direction as illustrated in Fig. 2(b) [35,36]. The electron ionized from the linearly polarized laser has almost zero p_z perpendicular to the laser polarization [37,38]. Thus, the measured three-peak structure can be attributed to the process of the linearly polarized pumping laser ionizing one electron to N_2O^+ and the elliptically polarized probing laser ionizing the other two electrons. The $p_{z\text{sum}}$ which can be fitted very well by using two Gaussian functions has a broad distribution for the high-KER band [as shown in Fig. 2(c)]. This corresponds to the process wherein the linearly polarized pump laser ionizes the molecules to dications and the third electron is released in the elliptically polarized laser field. These two Gaussian distributions indicate that the electron is ejected in the opposite direction in strong laser fields as illustrated in Fig. 2(c). Therefore, the time-dependent low-KER band can be assigned as the evolution of further ionization from N_2O^+ and the time-dependent high-KER band corresponds to the case from N_2O^{2+} . The lifetime of the fast decay for N_2O^+ is a little longer than the estimated lifetime of $B^2\Pi$ (~ 30 fs) [23]

but much shorter than the lifetime of $A^2\Sigma^+$ (on the order of nanoseconds) and $C^2\Sigma^+$ (~ 2 ps) states [24]. In addition, the excitation energy for $B^2\Pi$ is much smaller than that for the $C^2\Sigma^+$ state [24]. Therefore, the measured fast evolution of the low-KER band indicates that the dissociation most likely occurs from the $B^2\Pi$ state. The N_2O^{2+} is unstable even in the ground state $X^3\Sigma^-$, and the three lowest states ($X^3\Sigma^-$, $1^1\Delta$, and $1^1\Sigma^+$) dissociate to $\text{N}^+ + \text{NO}^+$ and higher states ($1^3\Pi$ and $1^1\Pi$) will dissociate to $\text{N}_2^+ + \text{O}^+$ by coupling with other states [21,31,39]. The $\text{N}^+ + \text{NO}^+$ channel is expected to contribute more in our measurement compared with the $\text{N}_2^+ + \text{O}^+$ channel due to accessible energy differences [27,39]. Furthermore, the three-body fragmentation occurs when the N_2O^{2+} populates to the high excited states [28,40].

The structure of the triatomic molecule N_2O after ionization can transform along the stretching and bending coordinate [26]. Figure 3 presents the mass-weighted Dalitz plots of the low-KER band at different delay times, which gives the three-body momentum correlations in the dissociation plane. The X axis is calculated with $(E_{\text{N}_2^+} - E_{\text{N}_1^+})/\sqrt{3}W$ and the Y axis is calculated with $E_{\text{O}^+}/W - 1/3$, where E_{O^+} , $E_{\text{N}_1^+}$, and $E_{\text{N}_2^+}$ are the measured kinetic energy of O^+ and two N^+ and W is the total KER of three ions. The Dalitz plots show that initially the linear molecule evolves to a triangular shape at 200 fs [Fig. 3(a i)] after populating to the $B^2\Pi$ state. The corresponding structure representation is shown in Fig. 3(b i). Observation indicates that significant bending takes place prior to the dissociation of N_2O^+ on the $B^2\Pi$ state, which qualitatively agrees with the previous observation that this molecular ion on the $B^2\Pi$ state will bend to about 70° relative to the linear structure of the ground state [19]. However, the structure bending is more significant in the current measurement than previous CE studies. Moreover, the Dalitz distribution becomes diffuse when the delay time increases from 400 fs to 1500 fs as shown in Figs. 3(a ii)–3(a v). The

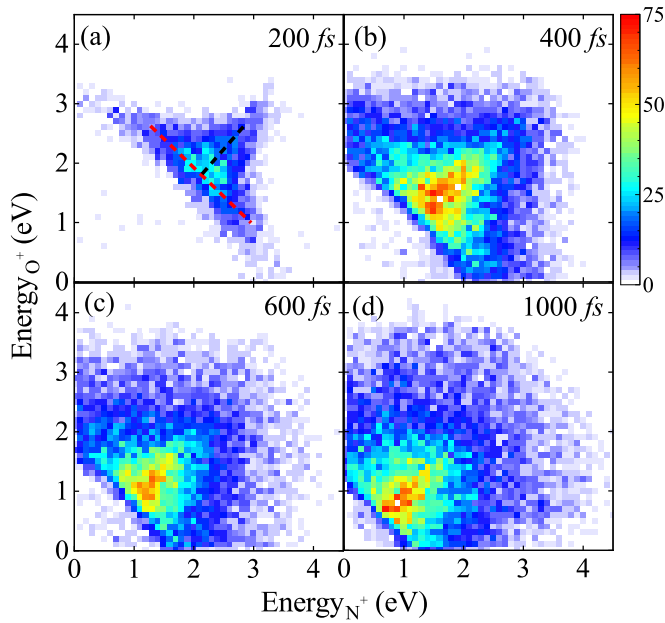


FIG. 4. Kinetic energy correlation diagrams for N^+ and O^+ ions generated from the further ionization and dissociation of N_2O^+ into $N^+ + N^+ + O^+$. The total KER is selected between 1.5 and 7 eV at four delay times: (a) 200 fs, (b) 400 fs, (c) 600 fs, and (d) 1000 fs.

Dalitz plots with the measured distribution subtracting the one obtained at a delay time of 200 fs after normalization to the same total signal intensity are shown in Figs. 3(b ii)–3(b v). The results reveal that the signal at the center of the Dalitz plot decreases and the outside signal with a triangular distribution increases with the delay time tuning from 200 fs to 1500 fs. The signals at the center of the Dalitz plot come from the concerted fragmentation in which three ions are breaking up at almost the same time. The triangular distribution can be assigned as the process of sequential dissociation because the kinetic energy sharing exists between two ions during the molecular fragmentation [28]. In the sequential process, the N_2O^+ first dissociates into $NO^+ + N$ or $N_2^+ + O$ after populated to the $B^2\Pi$ state and the further ionization leading to metastable NO^{2+} or N_2^{2+} . The transient fragments of NO^{2+} or N_2^{2+} can rotate before a sequential fragmentation step and the two ions produced break apart from the same fragments sharing the total kinetic energy from the CE of NO^{2+} or N_2^{2+} .

The concerted and sequential fragmentation process as well as the bond stretching can be deduced from the kinetic energy correlation of fragment ions [41]. We redraw the experimental data and show the kinetic energy correlation diagram of N^+ and O^+ at delay times of 200, 400, 600, and 1000 fs. The results are shown in Figs. 4(a)–4(d), respectively. A positive correlation corresponds to concerted fragmentation (black dashed line) and two ions sharing the total energy from a sequential process (red dashed line) are observed at a delay time of 200 fs as shown in Fig. 4(a). Furthermore, the correlation diagram becomes more diffusive as the delay time increases, which indicates that the correlation between ions becomes weaker as molecular bonds break, because the influence of neighbor atom on fragment ions becomes weaker as the distance between them increases. The KER of ions from

concerted fragmentation decreases as the delay time increases, which means the bond length between atoms is increasing during the dissociation. More importantly, the bond length of NO^+ also increases because the sharing energy between N^+ and O^+ decreases from 200 fs to 1000 fs as shown in Figs. 4(a)–4(d), which means the NO^+ is unstable. Thus, the decrease of the total KER with increasing delay time, which is expected, can be clearly observed in Fig. 2(a).

Now we will discuss the two-body and three-body dissociation of N_2O^{2+} . The two-body dissociation has two channels with $N^+ + NO^+$ and $O^+ + N_2^+$, while the three-body dissociation generates products of $N^+ + N + O^+$ and $N^+ + N^+ + O$. The Dalitz plots have been divided into two KER regimes at 7–12 and 12–16 eV as shown in Figs. 5(a) and 5(b), respectively. The Dalitz plots measured with the KER at 7–12 eV show a stripe structure and a triangular distribution marked by a red dashed line and three black dashed lines in Fig. 5(a i). The stripe structure corresponds to the fact that the O^+ has a high kinetic energy compared to the other two ions and its kinetic energy does not change (around 4 eV) as a function of delay time. The kinetic energy of N^+ decreases as the delay time increases, and two N^+ ions share the energy during the fragmentation. Thus, these ions can be assigned as generated from the two-body breakup process in which O^+ is released in the first step and N_2^+ is left in the excited vibrational states. vibrationally excited N_2^+ can dissociate via further ionization and lead to a lower kinetic energy at a longer delay time.

The measured triangular Dalitz distribution corresponds to the situation in which one of the ions has a lower kinetic energy compared to the other two ions as shown in Fig. 5(a). The relative energy of one ion decreasing as the delay time increases corresponds to the edge of the triangle moving close to the boundary of the Dalitz plots. The edge of the triangle comes from the sharing energy of two ions during fragmentation. This can be assigned as the further ionization of the three-body breakup from the dication, where the ion with low kinetic energy is generated from further ionization of the neutral atom. The three edges of the Dalitz distribution correspond to two three-body fragmentation processes ($N + N^+ + O^+$ and $N^+ + N^+ + O$). The bottom edge comes from the process of releasing one neutral O atom and two side edges come from the process of releasing a N atom during three-body fragmentation. The neutral atom flying far away before further ionization thus obtains a low energy from the repelling of the other two ions. The kinetic energy is around 1.5 eV for ions from further ionization of the neutral atom and the other two ions sharing the total kinetic energy around 7.5 eV at 400 fs. The other two ions are generated from the dication ionized by the pumping laser and the kinetic energy of these two ions are correlated.

The ions distributed in the center of the Dalitz plots with the KER between 12 and 16 eV are shown in Fig. 5(b). These can be assigned as the further fragmentation from the two-body channel $N^+ + NO^+$. The N^+ obtains kinetic energy around 5 eV during the two-body CE process, and the sequential fragmentation occurs after further ionization of NO^+ and generates N^+ and O^+ . The kinetic energies of N^+ (around 5 eV) and O^+ (around 4.5 eV) are from the CE of NO^{2+} with a total energy of about 9.5 eV. Therefore, three

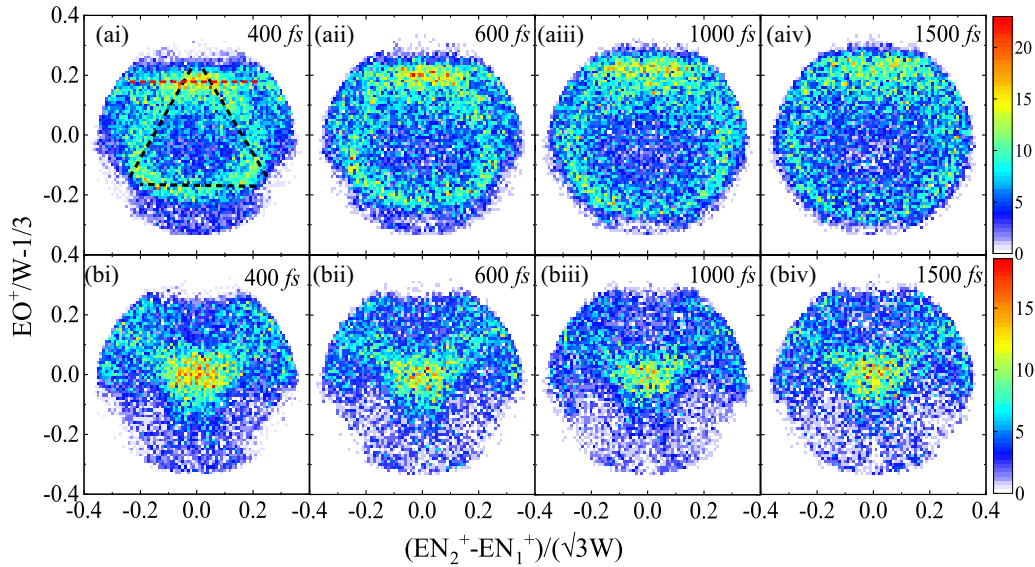


FIG. 5. Dalitz plot representation from the further ionization of N_2O^{2+} and subsequent dissociation of N_2O^{3+} into $N^+ + N^+ + O^+$, obtained by selecting the total KER (a) 7–12 eV and (b) 12–16 eV at delay times of (a i) and (b i) 400 fs, (a ii) and (b ii) 600 fs, (a iii) and (b iii) 1000 fs, and (a iv) and (b iv) 1500 fs.

of the ions from this process have almost the same kinetic energy, which leads to the center distribution of the Dalitz plots, and the signals extending to the edge of Dalitz plots are generated from the energy sharing between ions from the two-body dissociation process of molecules.

In order to further interpret the dissociation dynamics of N_2O^{2+} , the time-dependent kinetic energy correlation diagrams of N^+ and O^+ are shown in Fig. 6. The correlation diagrams for the KER in the ranges 7–12 and 12–16 eV are shown in Figs. 6(a) and 6(b), respectively. There are four noticeable correlations for low-KER ions marked by one red and three black dashed lines in Fig. 6(a ii), where the signal

along the black dashed lines shows no or weak correlation between N^+ and O^+ , while N^+ and O^+ ions have the energy correlation as marked by the red dashed line. Two kinds of energy correlation for the high-KER ions marked by red dashed lines and a red dashed circle are shown in Fig. 6(b). There are two dissociation pathways from further ionization of two-body breakup channels. The first pathway can be expressed as

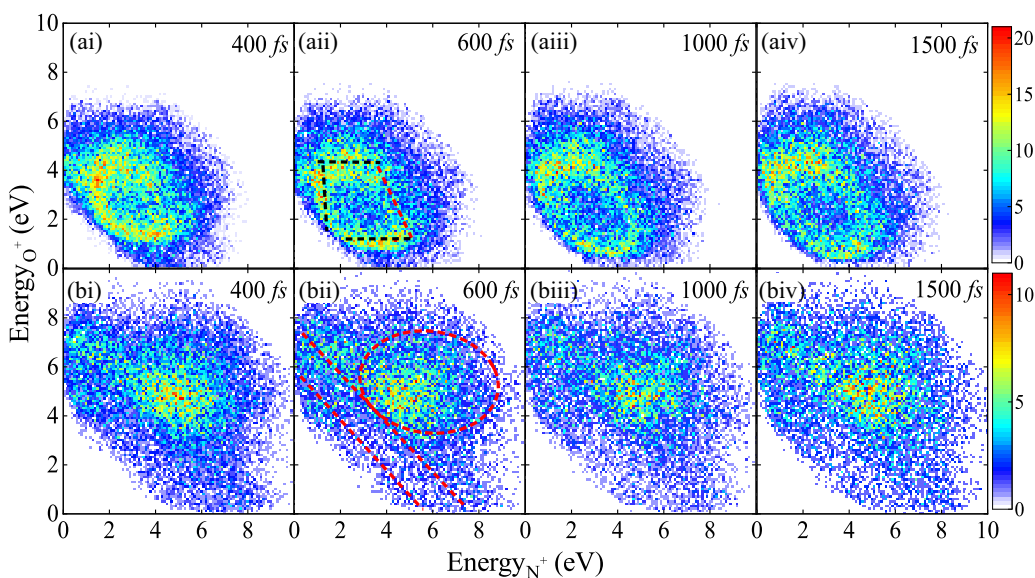
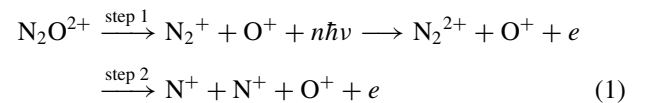
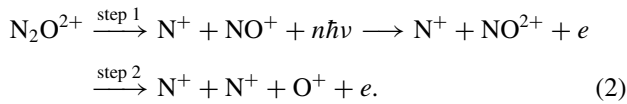


FIG. 6. (a) Kinetic energy correlation diagrams for N^+ and O^+ ions generated from the further ionization and dissociation of N_2O^{2+} into $N^+ + N^+ + O^+$ after selecting the total KER from 7 to 12 eV and (b) kinetic energy correlation diagrams for KER between 12 and 16 eV, after four delay times of (a i) and (b i) 400 fs, (a ii) and (b ii) 600 fs, (a iii) and (b iii) 1000 fs, and (a iv) and (b iv) 1500 fs.

and the second one is



The O^+ has no or weak correlation with the ejected N^+ from the first pathway, since the O^+ has departed from the molecule before the CE of N_2^{2+} . The O^+ leaves N_2O^{2+} in the first step and obtains the kinetic energy around 4 eV, which does not change as the delay time increases. This process can be assigned as the correlation distribution marked by the upper black dashed line in Fig. 6(a ii) and this also has been represented with the red dashed line of Fig. 5(a i). The kinetic energy of N^+ from the CE of N_2^{2+} can decrease to low energy due to the repelling of O^+ when one of the N^+ ions flies in the direction of O^+ . However, there are two correlation behaviors for N^+ and O^+ from the second two-body dissociation pathway because two N^+ ions from the CE of N_2O are indistinguishable in our measurement since they have the same mass-charge ratio. The ejected N^+ from first step has no or weak energy correlation with O^+ , while the N^+ from the second step has a strong correlation with O^+ because it breaks up from the same parent ion NO^{2+} . The kinetic energy shared between N^+ and O^+ is observed from dissociation of NO^{2+} as shown by the red dashed lines in Fig. 6(b ii). The signals with weak correlation between the first N^+ and O^+ are illustrated with the red dashed circle in Fig. 6(b ii), in which the correlation is different from the distribution from the dissociation pathway. This distribution may result from the NO^{2+} being a random distribution and the slow departing speed of ions before further fragmentation, thus the repelling of the first N^+ and O^+ leading to the broadened kinetic energy distribution of ions.

There are two pathways for three-body dissociation channels, which correspond to the ejection of O and N atoms. When the neutral O atom departs after the interaction of molecules with the pump laser, the O^+ gets very low energy and has no energy correlation with N^+ . This process corresponds to those ions marked with the lower black dashed line in Fig. 6(a ii). The energy of O^+ decreases from 1.5 eV at 400 fs to 0.5 eV at 1500 fs, as shown in Figs. 6(a i)–(a iv), because the bond between two N^+ ions and O is stretching after double ionization. The N^+ and O^+ ions sharing the total kinetic energy from three-body fragmentation accompany neutral N atoms, which are the observed correlations marked by the red dashed line. In contrast, the O^+ correlated with the N^+ from further ionization of the released N atom is marked by the left black line; this N^+ has a low kinetic

energy and shows weak correlation with O^+ . Since the neutral atom also has little impact on the ions released during three-body fragmentation, the distributions shown in the figures are not completely straight lines but are curved for three-body fragmentation channels. The energy correlation between N^+ and O^+ ions also weakly changes as the delay time increases from 400 fs to 1500 fs, as shown in Figs. 6(a i)–(a iv), because of the influence of the neutral atom decreasing as the delay time increases. The two-body and three-body fragmentation from double ionization have completely different influences on the energy correlation between fragments and ultrafast dissociation of molecules. However, it is difficult to completely distinguish the ions from these dissociation pathways because they have a very similar momentum distribution. These four distinguishable dissociation pathways demonstrate that fragmentation of triatomic molecule is very complicated, and the time-resolved three-body coincidence measurement presents a great perspective from which to disentangle the ultrafast dissociation dynamics of molecules in strong laser fields.

IV. CONCLUSION

We have performed the pump-probe experiment to track the nuclear movement of singly and doubly charged N_2O molecules triggered by strong field ionization. Two time-dependent KER spectra are observed and assigned as the corresponding evolution of N_2O^+ and N_2O^{2+} from the measured $P_{z\text{sum}}$ distributions. The time-resolved Dalitz distributions from the CE indicate that N_2O^+ undergoes a significant bending on the $B^2\Pi$ state. The differential Dalitz distributions and kinetic energy correlation between N^+ and O^+ at different delay times prove that the concerted breakup process dominates; however, the contribution of sequential fragmentation increases as the delay time increases. Two two-body and two three-body fragmentation pathways from N_2O^{2+} are resolved and the ultrafast dissociation of molecules and the energy correlation between ions from different dissociation pathways are tracked in real time. It is believed that the time-dependent coincidence measurements will open up avenues for the study of not only the static structure but also dynamic information of nonstationary states of even more complicated molecules.

ACKNOWLEDGMENTS

This work was supported by National Natural Science Foundation of China (Grants No. 11534004, No. 11704148, and No. 11627807) and the National Basic Research Program of China (Grant No. 2019YFA0307701).

- [1] T. Ergler, A. Rudenko, B. Feuerstein, K. Zrost, C. D. Schröter, R. Moshhammer, and J. Ullrich, *Phys. Rev. Lett.* **97**, 193001 (2006).
- [2] M. Magrakvelidze, O. Herrwerth, Y. H. Jiang, A. Rudenko, M. Kurka, L. Foucar, K. U. Kühnel, M. Kübel, N. G. Johnson, C. D. Schröter, S. Düsterer, R. Treusch, M. Lezius, I. Ben-Itzhak, R. Moshhammer, J. Ullrich, M. F. Kling, and U. Thumm, *Phys. Rev. A* **86**, 013415 (2012).

- [3] T. Okino, Y. Furukawa, Y. Nabekawa, S. Miyabe, A. A. Eilanlou, E. J. Takahashi, K. Yamanouchi, and K. Midorikawa, *Sci. Adv.* **1**, e1500356 (2015).
- [4] H. Ibrahim, B. Wales, S. Beaulieu, B. E. Schmidt, N. Thiré, E. P. Fowe, É. Bisson, C. T. Hebeisen, V. Wanie, M. Giguère, J. C. Kieffer, M. Spanner, A. D. Bandrauk, J. Sanderson, M. S. Schuurman, and F. Légaré, *Nat. Commun.* **5**, 4422 (2014).

- [5] N. G. Kling, S. D. Tendero, R. Obaid, M. R. Disla, H. Xiong, M. Sundberg, S. D. Khosravi, M. Davino, P. Drach, A. M. Carroll, T. Osipov, F. Marín, and N. Berrah, *Nat. Commun.* **10**, 2813 (2019).
- [6] S. De, M. Magrakvelidze, I. A. Bocharova, D. Ray, W. Cao, I. Znakovskaya, H. Li, Z. Wang, G. Laurent, U. Thumm, M. F. Kling, I. V. Litvinyuk, I. Ben-Itzhak, and C. L. Cocke, *Phys. Rev. A* **84**, 043410 (2011).
- [7] I. A. Bocharova, A. S. Alnaser, U. Thumm, T. Niederhausen, D. Ray, C. L. Cocke, and I. V. Litvinyuk, *Phys. Rev. A* **83**, 013417 (2011).
- [8] T. Ando, A. Iwasaki, and K. Yamanouchi, *Phys. Rev. Lett.* **120**, 263002 (2018).
- [9] Z. Wei, J. Li, L. Wang, S. T. See, M. H. Jhon, Y. Zhang, F. Shi, M. Yang, and Z. H. Loh, *Nat. Commun.* **8**, 735 (2017).
- [10] H. Akagi, T. Otobe, A. Staudte, A. Shiner, F. Turner, R. Dörner, D. M. Villeneuve, and P. B. Corkum, *Science* **325**, 1364 (2009).
- [11] P. Ma, C. Wang, X. Li, X. Yu, X. Tian, W. Hu, J. Yu, S. Luo, and D. Ding, *J. Chem. Phys.* **146**, 244305 (2017).
- [12] S. Luo, S. Zhou, W. Hu, X. Li, P. Ma, J. Yu, R. Zhu, C. Wang, F. Liu, B. Yan, A. Liu, Y. Yang, F. Guo, and D. Ding, *Phys. Rev. A* **96**, 063415 (2017).
- [13] H. Timmers, X. Zhu, Z. Li, Y. Kobayashi, M. Sabbar, M. Hollstein, M. Reduzzi, T. J. Martínez, D. M. Neumark, and S. R. Leone, *Nat. Commun.* **10**, 3133 (2019).
- [14] A. Hishikawa, A. Matsuda, M. Fushitani, and E. J. Takahashi, *Phys. Rev. Lett.* **99**, 258302 (2007).
- [15] Y. Malakar, W. L. Pearson, M. Zohrabi, B. Kaderiya, P. Kanaka, F. Ziaee, S. Xue, A. T. Le, I. Ben-Itzhak, D. Rolles, and A. Rudenko, *Phys. Chem. Chem. Phys.* **21**, 14090 (2019).
- [16] J. D. Burley, K. M. Ervin, and P. B. Armentrout, *J. Chem. Phys.* **86**, 1944 (1987).
- [17] D. R. Smith, E. R. Huppi, and J. O. Wise, *J. Atmos. Sol.-Terr. Phys.* **62**, 1189 (2000).
- [18] H. Xu, Y. Guo, Q. Li, S. Liu, X. Ma, J. Liang, and H. Li, *J. Chem. Phys.* **119**, 11609 (2003).
- [19] M. Lebeck, J. C. Houver, D. Dowek, and R. R. Lucchese, *J. Chem. Phys.* **120**, 8226 (2004).
- [20] H. Wang, X. Zhou, S. Liu, B. Jiang, D. Dai, and X. Yang, *J. Chem. Phys.* **132**, 244309 (2010).
- [21] X. Tang, M. Niu, X. Zhou, S. Liu, F. Liu, X. Shan, and L. Sheng, *J. Chem. Phys.* **134**, 054312 (2011).
- [22] G. Chambaud, H. Gritli, P. Rosmus, H. J. Wörner, and P. J. Knowles, *Mol. Phys.* **98**, 1793 (2000).
- [23] P. O. Danis, T. Wyttenbach, and J. P. Maier, *J. Chem. Phys.* **88**, 3451 (1988).
- [24] M. Lebeck, J. C. Houver, D. Dowek, and R. R. Lucchese, *J. Chem. Phys.* **117**, 9248 (2002).
- [25] X. Zhou, P. Ranitovic, C. W. Hogle, J. H. D. Eland, H. C. Kapteyn, and M. M. Murnane, *Nat. Phys.* **8**, 232 (2012).
- [26] M. Ueyama, H. Hasegawa, A. Hishikawa, and K. Yamanouchi, *J. Chem. Phys.* **123**, 154305 (2005).
- [27] M. Kübel, A. S. Alnaser, B. Bergues, T. Pischke, J. Schmidt, Y. Deng, C. Jendrzewski, J. Ullrich, G. G. Paulus, A. M. Azzeer, U. Kleineberg, R. Moshhammer, and M. F. Kling, *New J. Phys.* **16**, 065017 (2014).
- [28] K. Gope, I. Luzon, and D. Strasser, *Phys. Chem. Chem. Phys.* **21**, 13730 (2019).
- [29] R. Dörner, V. Mergel, O. Jagutzki, L. Spielberger, J. Ullrich, R. Moshhammer, and H. Schmidt-Böcking, *Phys. Rep.* **330**, 95 (2000).
- [30] J. Ullrich, R. Moshhammer, A. Dorn, R. Dörner, L. P. H. Schmidt, and H. Schmidt-Böcking, *Rep. Prog. Phys.* **66**, 1463 (2003).
- [31] S. Taylor, J. H. D. Eland, and M. Hochlaf, *J. Chem. Phys.* **124**, 204319 (2006).
- [32] C. Wang, X. Li, X.-R. Xiao, Y. Yang, S. Luo, X. Yu, X. Xu, L.-Y. Peng, Q. Gong, and D. Ding, *Phys. Rev. Lett.* **122**, 013203 (2019).
- [33] X. Li, J. Yu, H. Xu, X. Yu, Y. Yang, Z. Wang, P. Ma, C. Wang, F. Guo, Y. Yang, S. Luo, and D. Ding, *Phys. Rev. A* **100**, 013415 (2019).
- [34] P. Eckle, M. Smolarski, P. Schlup, J. Biegert, A. Staudte, M. Schöffler, H. G. Müller, R. Dörner, and U. Keller, *Nat. Phys.* **4**, 565 (2008).
- [35] A. N. Pfeiffer, C. Cirelli, M. Smolarski, R. Dörner, and U. Keller, *Nat. Phys.* **7**, 428 (2011).
- [36] J. Wu, L. P. H. Schmidt, M. Kunitski, M. Meckel, S. Voss, H. Sann, H. Kim, T. Jahnke, A. Czasch, and R. Dörner, *Phys. Rev. Lett.* **108**, 183001 (2012).
- [37] A. Rudenko, K. Zrost, T. Ergler, A. B. Voitkiv, B. Najjari, V. L. B. de Jesus, B. Feuerstein, C. D. Schörter, R. Moshhammer, and J. Ullrich, *J. Phys. B* **38**, L191 (2005).
- [38] D. Comtois, D. Zeidler, H. Pèpin, J. C. Kieffer, D. M. Villeneuve, and P. B. Corkum, *J. Phys. B* **38**, 1923 (2005).
- [39] L. Chen, X. Shan, X. Zhao, X. Zhu, X. Hu, Y. Wu, W. Feng, D. Guo, R. Zhang, Y. Gao, Z. Huang, J. Wang, X. Ma, and X. Chen, *Phys. Rev. A* **99**, 012710 (2019).
- [40] S. D. Price, J. H. D. Eland, P. G. Fournier, J. Fournier, and P. Millie, *J. Chem. Phys.* **88**, 1511 (1988).
- [41] C. Wu, C. Wu, D. Song, H. Su, Y. Yang, Z. Wu, X. Liu, H. Liu, M. Li, Y. Deng, Y. Liu, L.-Y. Peng, H. Jiang, and Q. Gong, *Phys. Rev. Lett.* **110**, 103601 (2013).